The Impact of Land–Atmosphere Interactions on the Temporal Variability of Soil Moisture at the Regional Scale

JOHN P. KOCHENDORFER AND JORGE A. RAMÍREZ

Department of Civil Engineering, Colorado State University, Fort Collins, Colorado

(Manuscript received 26 March 2004, in final form 10 August 2004)

ABSTRACT

This study examines the impact of the nonlinear dynamics of soil-moisture feedbacks to precipitation on the temporal variability of soil moisture at the regional scale. It is a modeling study in which the large-scale soil-water balance is first formulated as an ordinary differential equation and then recast as a stochastic differential equation by incorporating colored noise representing the high-frequency temporal variability and correlation of precipitation. The underlying model couples the atmospheric and surface-water balances and accounts for both *precipitation recycling* and *precipitation-efficiency feedbacks,* which arise from the surface energy balance. Based on the governing Fokker–Planck equation, three different analytical solutions (corresponding to differing forms and combinations of feedbacks) are derived for the steady-state probability density function of soil moisture. Using NCEP–NCAR reanalysis data, estimates of potential evapotranspiration, and long-term observations of precipitation, streamflow, and soil moisture, the model is parameterized for a $5^\circ \times 5^\circ$ region encompassing the state of Illinois. It is shown that precipitation-efficiency feedbacks can be significant contributors to the variability of soil moisture at the regional scale. Precipitation recycling, on the other hand, increases the variability by a negligible amount. For all feedback cases, the probability density function is unimodal and nearly symmetric. The analysis concludes with an examination of the dependence of the shape of the probability density functions on spatial scale. It is shown that the associated increases in either the correlation time scale or the variance of the noise will produce a bimodal distribution when precipitation-efficiency feedbacks are included. However, the magnitudes of the necessary increases are of an unrealistic magnitude.

1. Introduction

Since the seminal work of Charney et al. (1977), land-surface feedbacks have increasingly been recognized as significant sources of atmospheric variability. Soil moisture is perhaps the most important mediator of these feedbacks. In this paper, we examine the impact of land–atmosphere interactions on the temporal variability of regional-scale spatial averages of soil moisture. Our approach first formulates a large-scale, lumped-parameter water-balance model as an ordinary differential equation (ODE), with soil moisture as its state variable. To study the temporal variability in soil moisture in an analytical and probabilistic manner, we then recast the ODE as a stochastic differential equation (SDE) by adding colored noise that accounts for the high-frequency temporal variability and correlation of atmospheric moisture and precipitation efficiency. The underlying model of the coupled land–atmosphere water balance is formulated to capture both *precipitation recycling* and *precipitation-efficiency feedbacks*, which arise from the surface energy balance.

Our work here is based on that of Rodriguez-Iturbe et al. (1991), who used a lumped-parameter water-balance model formulated as an SDE to study continental-scale soil-moisture dynamics under the influence of land–atmosphere interactions. In their model, feedback from soil moisture to precipitation occurs through precipitation recycling only. In addition to including precipitation-efficiency feedbacks, our model also uses a fundamentally different relationship between atmospheric moisture and precipitation. A final important difference is that we use colored noise (rather than white noise, which is uncorrelated in time) to represent the high-frequency variability in advected atmospheric moisture. Wang et al. (1997) reformulated the original white-noise SDE of Rodriguez-Iturbe et al. (1991) to include colored noise. Our use of colored noise follows their general methodology. However, because our starting point is neither the same ODE nor a white-noise SDE, we arrive at necessarily and intrinsically different results.

For an example set of parameter values, Rodriguez-

Corresponding author address: Prof. Jorge A. Ramírez, Department of Civil Engineering, Colorado State University, Fort Collins, CO 80523-1372.
E-mail: Jorge.Ramirez@ColoState.edu

Iturbe et al. (1991) show that the probability density function (PDF) of soil-moisture transitions from unimodal to bimodal as the variance of the noise increases. Using the same model, Entekhabi et al. (1992) demonstrate the bimodal phenomenon for a hypothetical set of parameter values representing both semiarid and semihumid climates. Relative to the semihumid case, the bimodality in the PDF of soil moisture for the semiarid case is much less pronounced and occurs with much greater variance in the noise. Using a correlation time scale of 0.2 yr for the advected atmospheric moisture flux and the same parameter values in Rodriguez-Iturbe et al. (1991), Wang et al. (1997) find that their colored-noise solution enhances the bimodality in the PDF. As discussed in detail in Rodriguez-Iturbe et al. (1991) and Entekhabi et al. (1992), if a two-state dynamic exists in large-scale soil moisture, it would have profound implications for the persistence and variability of all components of the hydrological cycle. In particular, it may explain many of the multiyear droughts and pluvial periods observed over continental regions as oscillations within two distinct modes, with transitions between modes induced by ocean-controlled, low-frequency atmospheric variability.

Recycled precipitation has been shown to be a significant component of total precipitation at continental scales (e.g., Brubaker et al. 1993). Precipitation recycling, however, is somewhat of a misnomer in that moisture that refalls as precipitation does so mostly downwind of the point from where it evaporated. Consequently, the ratio of atmospheric moisture recycled from within the region to that derived from outside the region increases downstream. A spatially lumped model may thus be inappropriate for studying this feedback process at continental scales. One useful improvement to the model would be to add a downwind dimension along the lines of Savenije (1995). However, because we are confining our analysis to the regional scale, the spatially lumped form of the model is justifiable.

While precipitation recycling may not be significant at the regional scale, there is the possibility that other important feedbacks exist through the surface energy balance. The potential for these feedbacks exists because the energy balance at the surface controls atmospheric convection, and the energy balance is in turn controlled by soil moisture (with vegetation as an intermediary) through the Bowen ratio and surface albedo. Our model incorporates the aggregate effect of all such feedback mechanisms as a precipitation efficiency factor (which determines the fraction of input moisture flux that falls as precipitation) that is a nonlinear function of soil moisture. We thus refer to them as both precipitation-efficiency feedbacks and energy-balance feedbacks, depending on the context.

Using National Centers for Environmental Prediction (NCEP)–National Center for Atmospheric Research (NCAR) reanalysis data, estimates of potential evapotranspiration, and long-term observations of precipitation, streamflow, and soil moisture, we parameterize our model for the region bounded by 32.5°N, 42.5°N, 87.5°W, and 102.5°W (see Fig. 1). This 5° × 5° region encompasses all but the southern tip of Illinois. The Illinois State Water Survey (ISWS) has made observations of soil moisture using neutron probe techniques at 17 grass-covered sites across the state beginning as early as 1981 (Hollinger and Isard 1994). To our knowledge, no other in situ soil-moisture observation network at such a scale for such a length of time has existed in the United States. Consequently, the ISWS data and Illinois have been the focus of several research efforts dealing with the large-scale water balance and land–atmosphere interactions (e.g., Rodell and Famiglietti 2001; Brown and Arnold 1998; Eltahir and Yeh 1999; Findell and Eltahir 1997; Yeh et al. 1998). It is fortuitous for the latter type of study that Illinois has a semihumid climate and is located in a midlatitude, midcontinental region. As demonstrated by the general circulation modeling study of Koster et al. (2000), it is generally semihumid to semiarid climates and midlatitude, midcontinental regions where land surface feedbacks, relative to sea surface temperatures, have the greatest impact on the interannual variability of precipitation (and consequently soil moisture). In midlatitudes, potential evapotranspiration is generally of such a magnitude that, where humidity is in an intermediate range, evapotranspiration is both significant and highly

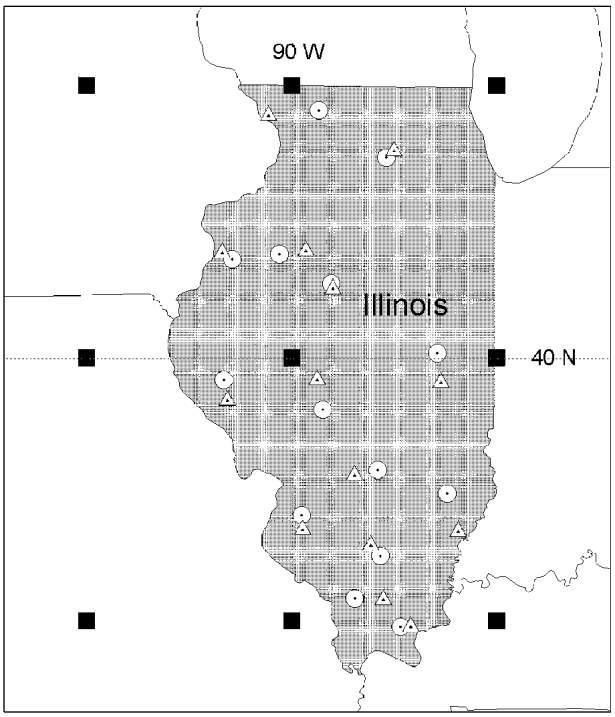

FIG. 1. Study region and data locations: NCEP–NCAR reanalysis grid points (black squares), ISWS soil-moisture stations (white circles), and USGS streamflow gauges (white triangles).

sensitive to soil moisture (i.e., predominantly under soil control, as opposed to climate control.) Because evapotranspiration—in the form of latent heat—is a component of the energy balance in addition to the water balance, precipitation-efficiency feedbacks are expected to be highly sensitive to soil moisture in the same regions as is precipitation recycling.

Land–atmosphere feedbacks that act through the energy balance are often associated with changes in vertical gradients of temperature and moisture in the atmospheric boundary layer. For example, Eltahir (1998) theorizes that soil moisture has a positive feedback to precipitation through the effect of the surface energy balance on large-scale vertical gradients in moist static energy. His theory is supported with both an analysis of observations from Kansas (Zheng and Eltahir 1998) and a modeling study of the drought of 1988 and the flooding of 1993 in the midwestern United States (Pal and Eltahir 2001), a domain that includes our study region. Through application of a regional climate model to several domains over Europe, Schär et al. (1999) show that significant differences in summertime convection result between uniformly dry and uniformly wet surface boundary conditions. In addition, there is a great deal of modeling and observational evidence for inhomogeneities in soil moisture and vegetation resulting in so-called sea-breeze circulations through *horizontal* gradients in temperature and moisture in the atmospheric boundary layer, as, for example, created by irrigation (Pielke and Zeng 1989) and other differences in land use and land cover. In our study region, there is a great deal of landscape patchiness created by agriculture fields and urbanization. In a study using satellite imagery, Brown and Arnold (1998) found a clustering of convective cloud cover along boundaries between differing land-cover types in Illinois during weak synoptic-scale flow. In addition, by comparison of that clustering with the ISWS soil-moisture data, they found that convective development occurred more often over the moister side of those boundaries. Although the mechanisms of feedbacks that act through the energy balance are undoubtedly multiple and complex, the evidence from the literature suggests that the net of all such feedbacks are positive over the entire observed range of soil moisture. Therefore, we assume that the mean precipitation efficiency is an increasing function of spatially averaged soil moisture.

2. Model development and analytical solutions

a. Deterministic differential equation governing the water balance

The differential equation governing the temporal evolution of soil-moisture content in the root zone is

$$n_e Z_r \frac{ds}{dt} = P(s)\phi(s) - E(s) - R_g(s), \tag{1}$$

where s is the degree of soil saturation (dimensionless), n_e is the effective soil porosity (dimensionless), Z_r is the depth of the root zone (L), $P(s)$ is the rainfall rate (L/T), $\phi(s)$ is the fraction of precipitation that infiltrates (dimensionless), $E(s)$ is the evapotranspiration rate (L/T), and $R_g(s)$ is the net runoff to groundwater, that is, percolation (L/T). Following Rodriguez-Iturbe et al. (1991), we write

$$E(s) = E_p s^{\varepsilon}, \tag{2}$$

$$\phi(s) = 1 - r_s s^{\rho_s}, \tag{3}$$

where E_p is the potential evapotranspiration rate (L/T) and ε, r_s, ρ_s are dimensionless constants. In parameterizing the model, it will be assumed that r_s takes on a value of either one or zero. When surface runoff is included, we want to ensure that the surface runoff ratio is unity for completely saturated soils (i.e., at $s = 1$). As demonstrated in the appendix, this condition is necessary for bounding the solution of the SDE at $s = 1$.

To the equation of Rodriguez-Iturbe et al. (1991), we have added a term for percolation to groundwater:

$$R_g(s) = Ks^{\rho_g}, \tag{4}$$

where K is the effective large-scale saturated hydraulic conductivity (L/T), and ρ_g is a dimensionless constant. In contrast to surface runoff and evapotranspiration (which are highly dependent on the dynamics of storm and interstorm periods), a power function for percolation to groundwater (by steady-state gravity drainage) is empirically and theoretically well established at a point scale (e.g., Brooks and Corey 1966).

For the equation governing the rainfall rate, we assume that total precipitation is proportional to the total input to the atmospheric moisture flux over the region. The two sources of input are moisture advected to the region and evapotranspiration from within the region. Formulating the former quantity for a two-dimensional land surface, we write

$$P(s) = h(s)[\mathrm{A} + E(s)], \tag{5}$$

where A is the moisture flux advected to the region per unit area of land surface (L/T), and h is the precipitation efficiency, that is, the fraction of input moisture flux which falls as precipitation. Schär et al. (1999) use the same equation, absent the explicit dependence on s, to determine precipitation efficiencies in the output of their regional climate model. We have included a dependence on s as a means of capturing energy-budget feedbacks as mediated by soil moisture. As is typical for a quantity defined as efficiency, h is theoretically limited to being no greater than one in the steady state. We use a power function for $h(s)$, as was done for $E(s)$, $R_g(s)$ and $\phi(s)$. Our equation for the precipitation rate as a function of soil moisture then becomes

$$P(s) = (\zeta + \eta s^{\theta})(\mathrm{A} + E_p s^{\varepsilon}), \tag{6}$$

where ζ, η and θ are non-negative constants (assuming a net positive feedback). Notice that s appears in two terms of (6). These terms represent energy-budget feedbacks and precipitation recycling, respectively. A constant is added to the power-law relationship in the precipitation efficiency function so that, in the case of completely dry soil (that is, $s = 0$), the precipitation efficiency is not zero. Setting η equal to zero will fix the precipitation efficiency at ζ, thereby removing the energy-budget feedbacks and leaving only precipitation recycling.

We substitute (2), (3), (4), and (6) into (1), divide by $n_e Z_r$, and normalize the atmospheric moisture flux by $\overline{A}$, the temporal mean of A, to arrive at a form of the differential equation for the water balance which involves only the time dimension:

$$ds/dt = a(\zeta + \eta s^{\theta})(\alpha + \beta s^{\varepsilon})(1 - r_s s^{\rho s}) - e_p s^{\varepsilon} - k s^{\rho g}, \tag{7}$$

where $a = \overline{A}/n_e Z_r$ (T^{-1}), $\alpha = A/\overline{A}$, $\beta = E_p/\overline{A}$, $e_p = E_p/n_e Z_r$ (T^{-1}), and $k = K/n_e Z_r$ (T^{-1}). α is a dimensionless measure of advected moisture flux and is the external driver of the system.

b. Colored-noise formulation of the stochastic differential equation

Conceptually, we can transform (7) from a deterministic to a stochastic differential equation by recognizing the existence of high-frequency variability (i.e., noise) in any of its three flux components. Precipitation undoubtedly contains the greatest amount of high-frequency variability, and so we add noise to this component only. The precipitation efficiency h and the atmospheric moisture flux α are both rapidly varying quantities. The former contains noise internal to the system, while the latter contains noise external to the system. We treat both α and h as the sums of a mean and a stochastic noise term:

$$\alpha = 1 + \sigma_\alpha \gamma_\alpha, \tag{8}$$

$$h(s) = \zeta + \eta s^{\theta} + \sigma_h(s)\gamma_h, \tag{9}$$

where σ_α is the standard deviation of α, $\sigma_h(s)$ is the standard deviation of h, and γ_α and γ_h are stochastic noise (all dimensionless). The mean of the noise in both equations is zero, and the standard deviation is one. It is also typical to assume that the noise in an SDE is Gaussian. Wang et al. (1997) show that this assumption is unnecessary for the governing Fokker–Planck equation (FPE) to be valid. Non-Gaussian noise is particularly useful for applications, such as the present, in which the noisy quantities take on only nonnegative values.

As will be seen in section 3d, the coefficient of variation of h appears to be independent of soil moisture. Therefore, we write

$$\sigma_h(s) = \nu_h(\zeta + \eta s^{\theta}), \tag{10}$$

where ν_h is the coefficient of variation of h. Substituting (2), (8), (9), and (10) into (5), along with $A = \alpha \overline{A}$ and $E_p = \beta \overline{A}$, we have

$$P(s, \gamma_\alpha, \gamma_h) = \overline{A}(\zeta + \eta s^{\theta})[\nu_h \sigma_\alpha \gamma_h \gamma_\alpha + (1 + \beta s^{\varepsilon})\nu_h \gamma_h + \sigma_\alpha \gamma_\alpha + 1 + \beta s^{\varepsilon}]. \tag{11}$$

For the purpose of analytical tractability, we would like to combine the two noise components, γ_α and γ_h, into a single, composite noise. A complicating factor is the product of $(1 + \beta s^{\varepsilon})$ and γ_h in (11). If the second term in the former is always small relative to one (which is equivalent to assuming that the evaporative flux is small relative to the mean of the input moisture flux), we can ignore its variability and replace s by $\bar{s}$, its temporal mean. Provided that the PDF of s is not heavily skewed, a reasonable a priori estimate of $\bar{s}$ is the deterministic steady state, which can be found by setting (7) equal to zero. In section 3, we estimate a value for β of 0.087. Given that the maximum value of s is one, we can conclude that βs^{ε} will always be less than 0.087. Under the assumption that s is stationary in the second term in the brackets of (11), we define a new random variable,

$$\begin{aligned} \Gamma &= \nu_h \sigma_\alpha \gamma_h \gamma_\alpha + (1 + \beta \bar{s}^{\varepsilon})\nu_h \gamma_h + \sigma_\alpha \gamma_\alpha \\ &= \mu + \sigma \gamma, \end{aligned} \tag{12}$$

where γ is the composite noise (with zero mean and unit variance), and μ and σ are the mean and standard deviation of Γ. (11) can then be rewritten as

$$P(s, \gamma) = \overline{A}(\zeta + \eta s^{\theta})(\mu + \sigma\gamma + 1 + \beta s^{\varepsilon}). \tag{13}$$

Using basic principles for the addition and multiplication of random variables (Benjamin and Cornell 1970), it can be shown that

$$\sigma \approx [(1 + \nu_h^2)\sigma_\alpha^2 + (1 + \beta \bar{s}^{\varepsilon})^2 \nu_h^2 + 2(1 + \beta \bar{s}^{\varepsilon})\nu_h \sigma_\alpha \operatorname{Cov}[\gamma_\alpha, \gamma_h]]^{1/2} \tag{14}$$

$$\mu = \nu_h \sigma_\alpha \operatorname{Cov}[\gamma_\alpha, \gamma_h], \tag{15}$$

where $\operatorname{Cov}[\gamma_\alpha, \gamma_h]$ is the covariance of γ_α and γ_h. Including covariance between h and α captures a presumed dependence of precipitation efficiency on the external input of moisture (and associated latent heat).

Replacing the deterministic form of precipitation in (7) with the stochastic formulation, (13), allows us to write an SDE of the Langevin form (Gardiner 1985):

$$ds_t/dt = \Delta(s_t) + \sigma\delta(s_t)\,\gamma_t, \tag{16a}$$

where $\Delta(s_t)$ is the drift function, and $\sigma\delta(s_t)$ is the diffusion function. These functions are defined in our model by

$$\Delta(s) = a(\mu + 1 + \beta s^{\varepsilon})(\zeta + \eta s^{\theta})(1 - r_s s^{\rho s}) - e_p s^{\varepsilon} - k s^{\rho g}, \tag{16b}$$

$$\delta(s) = a(\zeta + \eta s^{\theta})(1 - r_s s^{\rho s}). \tag{16c}$$

The use of the terms *drift* and *diffusion* dates from the original application of stochastic calculus to the study of Brownian motion and other diffusion processes. The subscript t is used in the usual sense to indicate the stochastic time dependence of a quantity. As in (16b)–(16c) we will frequently drop the subscript for the sake of notational parsimony, especially when time is not explicitly part of the equation.

Both α and h are temporally correlated, and so γ also possesses temporal correlation. In other words, we need to treat the noise in our SDE as colored, as opposed to more commonly used white noise, which is uncorrelated in time. One approach to coloring the noise in an SDE is to treat the noise as being generated by the Ornstein–Uhlenbeck process (e.g., Wang et al. 1997; Høyrup 1996). The origin of the Ornstein–Uhlenbeck process is in Langevin's model of Brownian motion (Gardiner 1985) in which the velocity (rather than the position) of the particle is the principal stochastic variable subject to a white-noise forcing. The result is that the velocity is no longer nondifferentiable in time and thus possesses temporal correlation. Conceptualizing γ as velocity in the Ornstein–Uhlenbeck process, we can write an SDE for γ of the form

$$d\gamma_t = -\frac{1}{\tau}\gamma_t dt + \sqrt{D}\, dW_t, \tag{17}$$

where τ is the correlation time scale of γ, D is the diffusion coefficient, and dW_t is the derivative of the Weiner process (Gardiner 1985). The Weiner process is the stochastic integration of white noise. Gardiner (1985) shows that, in the steady state,

$$\mathrm{Var}[\gamma_t] = \frac{D\tau}{2}, \tag{18}$$

$$\mathrm{Cov}[\gamma_{t_1}, \gamma_{t_2}] = \frac{D\tau}{2} e^{-|t_1 - t_2|/\tau}. \tag{19}$$

In order that (18) and (19) both equal unity when $t_1 = t_2$,

$$D = \frac{2}{\tau}. \tag{20}$$

The autocovariance functions of the three noise-containing terms in (11) can be aggregated in the same manner as the variances. If the correlation time scales of γ_α and γ_h are of the same order of magnitude, the autocovariance function of γ can be approximated well as exponential by equating the autocorrelation function of the composite noise with (19) at $t_1 - t_2 = \tau$. This gives

$$\frac{\sigma^2}{e} = (1 + \beta\bar{s}^{\varepsilon})^2 \nu_h^2 e^{-\tau/\tau_h} + \sigma_\alpha^2 e^{-\tau/\tau_\alpha} + \nu_h^2 \sigma_\alpha^2 e^{-\tau(\tau_\alpha + \tau_h)/\tau_\alpha \tau_h} + (1 + \beta\bar{s}^{\varepsilon})\nu_h \sigma_\alpha \,\mathrm{Cov}[\gamma_\alpha, \gamma_h](e^{-\tau/\tau_{\alpha,h}} + e^{-\tau/\tau_{h,\alpha}}), \tag{21}$$

where τ_α and τ_h are the correlation time scales of γ_α and γ_h, respectively, and $\tau_{\alpha,h}$ and $\tau_{h,\alpha}$ are the cross-correlation time scales of γ_α and γ_h. τ can then be solved for numerically using (21).

Solving for γ in (16a) and substituting the result into (17) along with (20) yields

$$\frac{d}{dt}\left[\frac{1}{\sigma\delta(s)}\left(\frac{ds}{dt} - \Delta(s)\right)\right] = -\frac{1}{\tau}\left[\frac{1}{\sigma\delta(s)}\left(\frac{ds}{dt} - \Delta(s)\right)\right] + \sqrt{\frac{2}{\tau}}\frac{dW}{dt}. \tag{22}$$

Differentiating the left-hand side (lhs) of (22) and rearranging gives

$$\frac{d^2 s}{dt^2} = \frac{1}{\delta(s)}\frac{\partial\delta(s)}{\partial s}\left(\frac{ds}{dt}\right)^2 + \left[\delta(s)\frac{\partial}{\partial s}\left(\frac{\Delta(s)}{\delta(s)}\right) - \frac{1}{\tau}\right]\frac{ds}{dt} + \frac{\Delta(s)}{\tau} + \sqrt{\frac{2}{\tau}}\sigma\delta(s)\frac{dW}{dt}. \tag{23}$$

As a simplifying approximation, we discard the squared and second-derivative terms (i.e., the higher-order terms) to arrive at

$$ds = \frac{\Delta(s)dt + \sqrt{2\tau}\sigma\delta(s)dW}{1 - \tau\delta(s)\dfrac{d}{ds}\left(\dfrac{\Delta(s)}{\delta(s)}\right)}. \tag{24}$$

We define new drift and diffusion terms,

$$A(s) = \frac{\Delta(s)}{1 - \tau\delta(s)\dfrac{d}{ds}\left(\dfrac{\Delta(s)}{\delta(s)}\right)}, \tag{25a}$$

$$\sqrt{B(s)} = \frac{\sqrt{2\tau}\sigma\delta(s)}{1 - \tau\delta(s)\dfrac{d}{ds}\left(\dfrac{\Delta(s)}{\delta(s)}\right)} \tag{25b}$$

in order to write (24) in another standard form of the Langevin equation (Gardiner 1985):

$$ds_t = A(s_t)dt + \sqrt{B(s_t)}dW_t. \tag{25c}$$

The time evolution of the PDF of s is governed by the Ito FPE (Gardiner 1985),

$$\frac{\partial}{\partial t} f_S(s_t, t) = -\frac{\partial}{\partial s}[A(s_t) f_S(s_t, t)] + \frac{1}{2}\frac{\partial^2}{\partial s^2}[B(s_t) f_S(s_t, t)], \tag{26}$$

where $f_S(s_t, t)$ is the PDF of s at time t.

c. *Steady-state solution of the Fokker–Planck equation*

Under steady-state conditions, the lhs of (26) equals zero, and $f_S(s_t, t) = f_{ss}(s)$ (where the first subscript is the variable s, and the second subscript indicates the steady state), with the solution (Gardiner 1985)

$$f_{S_s}(s) = \frac{C}{B(s)} \exp\left[2 \int_0^s \frac{A(x)}{B(x)}\, dx \right], \tag{27a}$$

where C is a normalization constant such that

$$\int_0^1 f_{S_s}(s) ds = 1. \tag{27b}$$

We now consider the existence and form of a general, analytical solution for (27a). None was found for the general forms of $\Delta(s)$ and $\delta(s)$. However, when the exponents θ, ε, ρ_s, and ρ_g assume whole or half integer values, a particular solution usually can be found. In addition, when ζ is set equal to zero, a solution exists for all values of the exponents. Even with $\zeta = 0$, the solution consists of a large number of infinite series sums. If we assume that τ is on the order of a few days or less, and that the surface runoff ratio is small—generally a reasonable assumption for all but the most humid climates and steep terrain—we can approximate the denominators in (25a)–(25b) as one (see the appendix). With this approximation, (27a) becomes

$$f_{S_s}(s) = \frac{C}{2\tau\sigma^2 \delta^2(s)} \exp\left[\frac{1}{\tau\sigma^2} \int_0^s \frac{\Delta(x)}{\delta^2(x)}\, dx \right]. \tag{28}$$

If we assume all precipitation infiltrates by setting r_s equal to zero (see the appendix), (28) evaluates to

$$f_{S_s}(s) = \frac{C}{2\tau\sigma^2(\zeta + \eta s^\theta)^2} \exp\left\{ \frac{1}{\tau\sigma^2} \left[(1+\mu)\, s \sum_{n=0}^{\infty} \frac{\left(\frac{-\eta s^\theta}{\zeta} \right)^n}{\frac{1}{\theta} + n} + \sum_{i=1}^{3} \left\{ U_i s^{V_i} \left[\frac{\zeta}{\zeta + \eta s^\theta} + (\theta - V_i) \right] \sum_{n=0}^{\infty} \frac{\left(\frac{-\eta s^\theta}{\zeta} \right)^n}{\frac{V_i}{\theta} + n} \right\} \right] \right\}, \tag{29a}$$

where

$$\mathbf{U}_\mathrm{T} = \left[\frac{a\zeta\beta - e_p}{a\zeta}, -\frac{k}{a\zeta}, \frac{\eta\beta}{\zeta} \right], \tag{29b}$$

$$\mathbf{V}_\mathrm{T} = [\varepsilon + 1, \rho_g + 1, \theta + \varepsilon + 1]. \tag{29c}$$

If in addition $\zeta = 0$, the integration in (28) leads to

$$f_{S_s}(s) = \frac{C}{2\tau\sigma^2\eta^2 s^{2\theta}} \exp\left\{ \frac{s^{1-\theta}\left[\frac{(\mu+1)}{1-\theta} - \frac{k s^{\rho_g}}{a\eta s^\theta (1 - 2\theta + \rho_g)} + s^\varepsilon \left(\frac{\beta}{1 - \theta + \varepsilon} - \frac{e_p}{a\eta s^\theta (1 - 2\theta + \varepsilon)} \right) \right]}{\tau\sigma^2 a\eta} \right\} \tag{30}$$

with the constraints $\theta \neq 1$, $\theta - \varepsilon \neq 1$, $2\theta - \varepsilon \neq 1$, and $2\theta - \rho_g \neq 1$. As a final case, if $\eta = 0$, (29) reduces to

$$f_{S_s}(s) = \frac{C}{2\tau\sigma^2\zeta^2} \exp\left\{ \frac{s\left[a\zeta\left(\mu + 1 + \frac{\beta s^\varepsilon}{1+\varepsilon} \right) - \frac{k s^{\rho_g}}{1+\rho_g} - \frac{e_p s^\varepsilon}{1+\varepsilon} \right]}{\tau\sigma^2 a^2 \zeta^2} \right\}. \tag{31}$$

The first two cases [i.e., Eqs. (29) and (30)] are those with precipitation-efficiency feedbacks and precipitation recycling, while the third [i.e., Eq. (31)] captures only the latter. A fourth case with no feedbacks at all can be had by setting β equal to zero in (31).

3. Estimation of parameter values for the study region

a. Soil moisture

Monthly, spatial averages of s were calculated using data from the 14 ISWS stations (see Fig. 1) that both began measurements in 1983 and are located in the dominant silt-loam soils. The data are currently available through November 2001 from the Global Soil Moisture Databank (Robock et al. 2000), making for a total of 227 months. An important aspect to vertically averaging the soil-moisture data is selection of an averaging depth. We want to measure s over the depth that responds to high-frequency atmospheric variability. This is often assumed to be the depth of the root zone, Z_r. Root density typically decreases asymptotically with depth (Jackson et al. 1996), and so a single value for root depth is often difficult to determine. An

alternative approach is to examine the coefficients of variation in soil-moisture content as a function of depth. For the 14 ISWS sampling locations, the coefficients of variation generally decrease with depth in an exponential fashion with most of the variability damped out at about the 70–90-cm sampling interval. Therefore, a value of 90 cm was selected for Z_r. The mean effective soil porosity for the soils was estimated as 0.48, resulting in a value of $n_e Z_r$ of 43 cm. The vertically averaged values of s were then averaged within each month, followed by an averaging across stations to obtain a single statewide average for each month.

b. Precipitation

Monthly precipitation estimates for the study region were extracted from a monthly dataset generated by the PRISM model (Daly et al. 1994) for the Vegetation/Ecosystem Modeling and Analysis Project (VEMAP; available online at http://www.cgd.ucar.edu/vemap/). These data cover the lower 48 states at a 0.5° resolution and span the period 1895–1993. In addition, daily precipitation data from the National Oceanic and Atmospheric Administration (NOAA) Climate Prediction Center (CPC; Higgins et al. 2000) as made available by the NOAA–Cooperative Institute for Research in Environmental Sciences (CIRES) Center for the Diagnosis of Climate (CDC; available online at http://www.cdc.noaa.gov/cdc/data.unified.html) were used in the calculation of daily values of h as described below in section 3d. These data cover the lower 48 states at a 0.25° resolution over the period 1948–97. Aggregated to the monthly scale for the study region, they agreed extremely well with the PRISM data ($R^2 > 0.99$). The 11-yr overlap (1983–93) of the VEMAP and ISWS data was selected as the parameterization period. Table 1 lists all parameter values, the derivation of which is further detailed below.

TABLE 1. Parameter values for the study region.

Parameter	Value		
Storage capacity of root zone, $n_e Z_r$ (mm)	430		
Temporal mean of s, $\bar{s}$	0.68		
Mean advected moisture flux, $\overline{A}$ (mm day^{-1})	34.1		
Standard deviation of α, σ_α	0.697		
Coefficient of variation of h, ν_h	1.24		
Covariance of γ_α and γ_h, Cov[γ_α, γ_h]	0.24		
Correlation time scale of γ_α, τ_α (days)	1.77		
Correlation time scale of γ_h, τ_h (days)	0.87		
Cross-correlation time scale of γ_α and γ_h $\tau_{\alpha h}$ (days)	2.1		
Cross-correlation time scale of γ_h and γ_α, $\tau_{h,\alpha}$ (days)	0.50		
Mean of composite noise, μ	0.207		
Standard deviation of composite noise, σ	1.84		
Correlation time scale of composite noise, τ	0.89		
Precipitation-efficiency constant, ζ	0.064	0	0.033
Precipitation-efficiency coefficient, η	0	0.091	0.067
Precipitation-efficiency exponent, θ	NA	0.9	2
Infiltration function coefficient, r_s	0		1
Infiltration function exponent, ρ_s	NA		7.9
Effective saturated hydraulic conductivity, K (mm day^{-1})	7.1		4.2
Groundwater runoff function exponent, ρ_g	6.2		5.7
Potential evapotranspiration rate, E_p (mm day^{-1})	2.96		
Ratio of E_p to $\overline{A}$, β	0.087		
Evapotranspiration function exponent, ε	1.2		

c. Surface runoff, groundwater runoff, and evapotranspiration

Daily data from U.S. Geological Survey stream gauges (available online at http://water.usgs.gov/nwis/discharge) were used to estimate monthly runoff over the parameterization period. To minimize routing times and to offset sampling bias in the soil-moisture data, 14 small river basins were identified that contain, or are near, the soil-moisture sampling locations (see Fig. 1 for locations of gauges). To divide total streamflow into storm flow and base flow, we used the hydrograph separation methodology of Woodruff and Hewlett (1970). The resulting average surface runoff ratio was found to be 0.13. Two sets of values for K and ρ_g, one under the assumption that all streamflow is groundwater runoff ($r_s = 0$) and one with surface runoff included ($r_s = 1$), were determined via a log–log regression of (4) (see Figs. 2a,b). Likewise, a value for ρ_s in the case of $r_s = 1$ was determined via a log–log regression of the surface runoff ratio versus soil moisture (see Fig. 2c). As evidenced by the distinction made in Fig. 2 between months of decreasing (March–August) and increasing (September–February) groundwater storage, estimates of groundwater runoff are subject to significant storage effects. It is assumed, however, that months of increasing storage will offset months of decreasing storage in the regression.

Annual values of evapotranspiration were estimated as the difference between precipitation and streamflow. Annual values were used because changes in vadose-zone and groundwater storage are too significant at the monthly scale. As long as ε in (2) does not deviate much from unity, the annual scale should provide a reasonable approximation of the exponent. As shown in Fig. 3, a regression of $\log(E/E_p)$ versus $\log(s)$ produced a value for ε of 1.2, with an R^2 of 0.52. Estimates of annual potential evapotranspiration were aggregated from monthly estimates, which were calculated using the Penman equation (Penman 1948) as presented by Shuttleworth (1993). Inputs to the Penman equation where derived mainly from the VEMAP

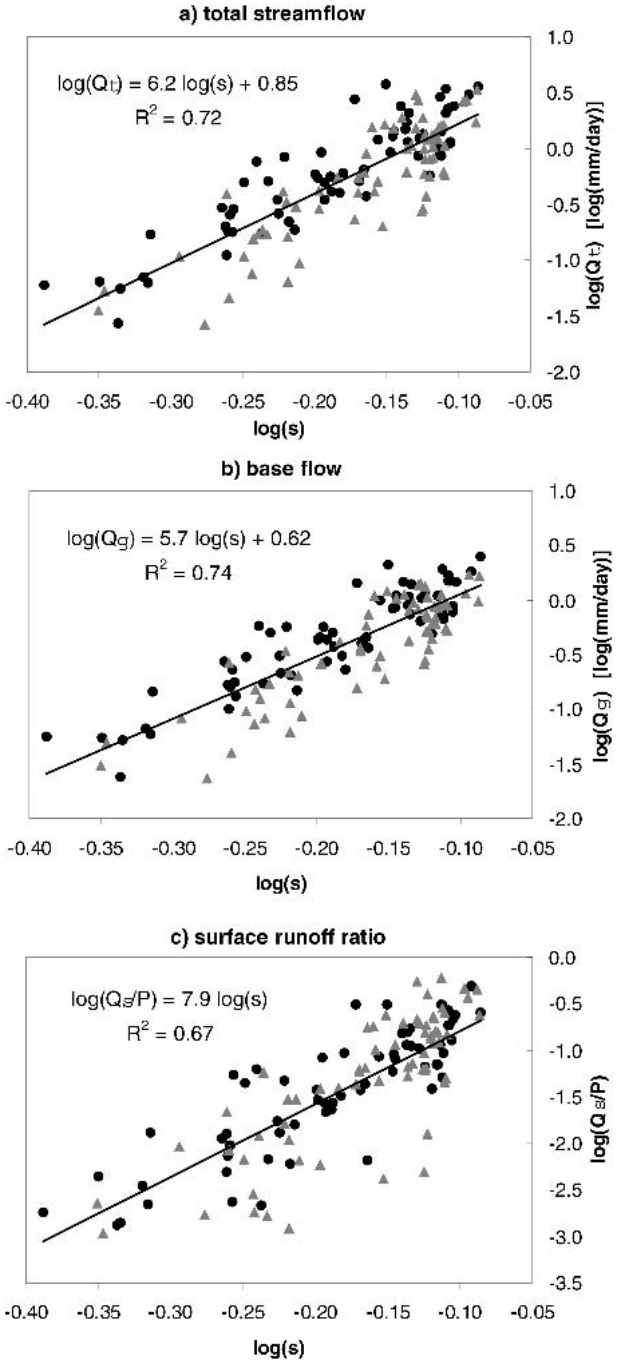

FIG. 2. Log–log regressions of monthly streamflow vs soil moisture (1983–93): (a) total streamflow, (b) base flow, and (c) surface runoff ratio. Black circles are months of decreasing soil and groundwater storage (Mar–Aug). Gray triangles are months of increasing storage (Sep–Feb). The regressions are for all months.

dataset, with exception of surface wind speed, which was derived from NCEP–NCAR reanalysis data, and surface albedo, which was taken from a gridded, monthly climatology developed by Hobbins et al. (2001).

d. Atmospheric moisture flux and precipitation efficiency

Results from the NCEP–NCAR reanalysis project (Kalnay et al. 1996) as provided by NOAA–CIRES CDC (available online at http://www.cdc.noaa.gov/cdc/reanalysis/) were the source of wind speed, specific-humidity, and surface-pressure data. These data are at a 6-h time step and are resolved vertically by 14 pressure levels and horizontally at 2.5° latitude and longitude. Thus eight grid points bound the study region, with a single grid point at the center (see Fig. 1). At each of these nine grid points, the meridional and zonal components of the horizontal moisture flux were vertically integrated via linear interpolation of wind and specific humidity and truncation at the surface pressure. The general form of this integration is

$$F_{u,v} = \frac{p_s}{g} \int_{p_s}^{0} w_{u,v}(p)\, q(p)\, dp, \tag{32}$$

where $F_{u,v}$ are the horizontal moisture flux components ($ML^{-1}T^{-1}$), p_s is the surface pressure ($ML^{-1}T^{-2}$), g is the acceleration due gravity (LT^{-2}), p is the atmospheric pressure ($ML^{-1}T^{-2}$), $w_{u,v}$ are the wind components (LT^{-1}), and q is the specific humidity (dimensionless). Daily values of $F_{u,v}$ for the study region were obtained by taking the mean of the 6-h values at each grid point and then averaging across the nine grid points, weighting each by the fraction of the study region it represents. We divided the two flux components by the respective downwind length of the study region and the density of water to arrive at the desired dimensions of LT^{-1}, where the length dimension represents water depth. The magnitude of the vector sum of the two components gives a single value, F_A, for the mean atmospheric moisture flux over the study region.

Using the analogy of a streamtube with uniform precipitation and evapotranspiration down its length (e.g.,

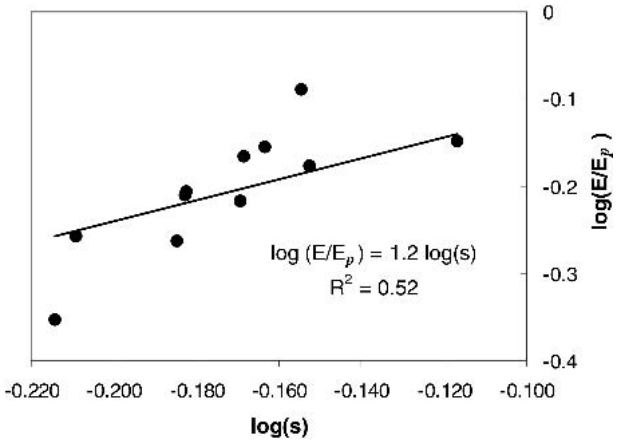

FIG. 3. Log–log regression of the ratio of annual evapotranspiration to potential evapotranspiration vs annual mean soil moisture (1983–93).

Entekhabi et al. 1992; Budyko 1974), it can be shown that

$$A = F_A - \frac{(E - P)}{2}. \tag{33}$$

Thus, to obtain daily values of A, we also need daily values of E. From an atmospheric water balance,

$$E = P + \nabla \cdot \mathbf{F} + dW_a/dt, \tag{34}$$

where $\nabla \cdot \mathbf{F}$ is the divergence of atmospheric moisture from the region (LT^{-1}) and dW_a/dt is the rate of change of moisture stored in the atmosphere above the region (LT^{-1}). Via comparison to a surface water balance, Yeh at al. (1998) show that use of (34) with the NCEP–NCAR reanalysis data provides a reasonably accurate monthly climatology of E for the study region, but that there are significant errors to estimates for individual months [hence the reason such estimates were not used in the parameterization of (2)]. Undoubtedly, daily estimates calculated with (34) will be even more inaccurate. Both the analysis of Yeh et al. and our own suggest that the accuracy of reanalysis-based evapotranspiration estimates decreases with decreasing size of the region. Fortunately, A—and thus its contribution to the moisture flux relative to E—is inversely proportional to the downwind length of the region. For the study region, maximum evapotranspiration occurs in July, for which we estimated a mean value of E of 4.2 mm day^{-1}, which is only about 10% of the July mean of A. Therefore, we can immediately conclude that evapotranspiration from within the region contributes minimally to the average atmospheric moisture flux over the study region. The impact this has on the variability of soil moisture is seen in section 4.

Daily values of α were calculated by dividing the daily values of A by the annual harmonic in the means of A. As per (5), dividing daily precipitation by the daily estimates of $A + E$ provides daily values of h for the period 1983–93. In this 11-yr period, there are only 70 days in the CPC precipitation data when all of the grid cells comprising the study region are assigned zero precipitation. The study region thus appears to be large enough that the spatial average of daily precipitation—and hence h—can be modeled as a continuous process. To investigate the dependence of the standard deviation of h on s, we averaged the standard deviation and mean within each month. Those values are plotted against each other in Fig. 4 for the 132 months in the parameterization period. Based on the correlation between the two quantities, and assuming that s is relatively invariant within a given month, it appears that the standard deviation has the same dependence on s as does the mean; that is, the coefficient of variation is independent of s. We use the slope of the regression line in Fig. 4 as the coefficient of variation of h.

The next parameter values that we determine are the

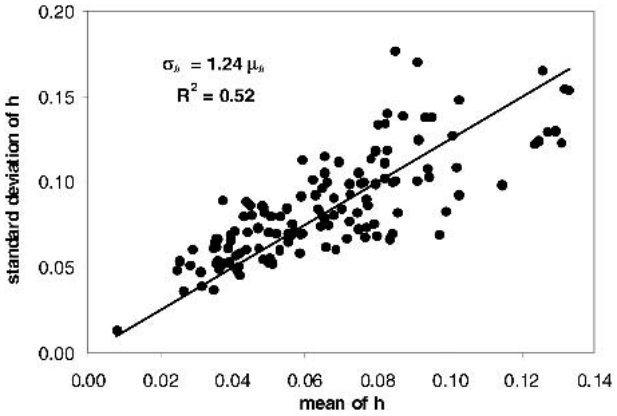

FIG. 4. Mean vs standard deviation of daily precipitation efficiencies within each month (1983–93). Line and equation are results of zero-intercept least squares regression.

covariance and correlation time scales of γ_α and γ_h. Daily values of α versus h are plotted in Fig. 5. Only a low amount of positive correlation is evident in the plot, particularly at higher values. The correlation coefficient between α and h, which is approximately equal to the covariance of γ_α and γ_h, is 0.24. Autocorrelation and cross-correlation coefficients of the daily values of α and h are plotted in Fig. 6. Fits to exponential autocorrelation functions were performed via least squares regression on a natural log transform of the values of the correlation coefficients up to and including the first value below 0.05. The cutoff was selected as a compromise between statistical significance and the need for an adequate number of points. The corresponding values of τ_α and τ_h are 1.79 and 0.86 days, respectively. Such correlation time scales are consistent with the passing of synoptic-scale fronts. With the parameters of α and h and their associated noise components determined, we apply (13), (15), and (21) to arrive at values for the

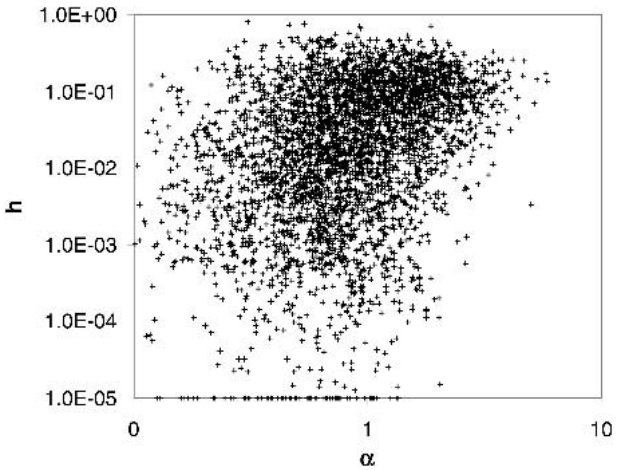

FIG. 5. Normalized daily advected moisture flux vs precipitation efficiency (1983–93). Values of h less than 10^{-5} are plotted at 10^{-5}.

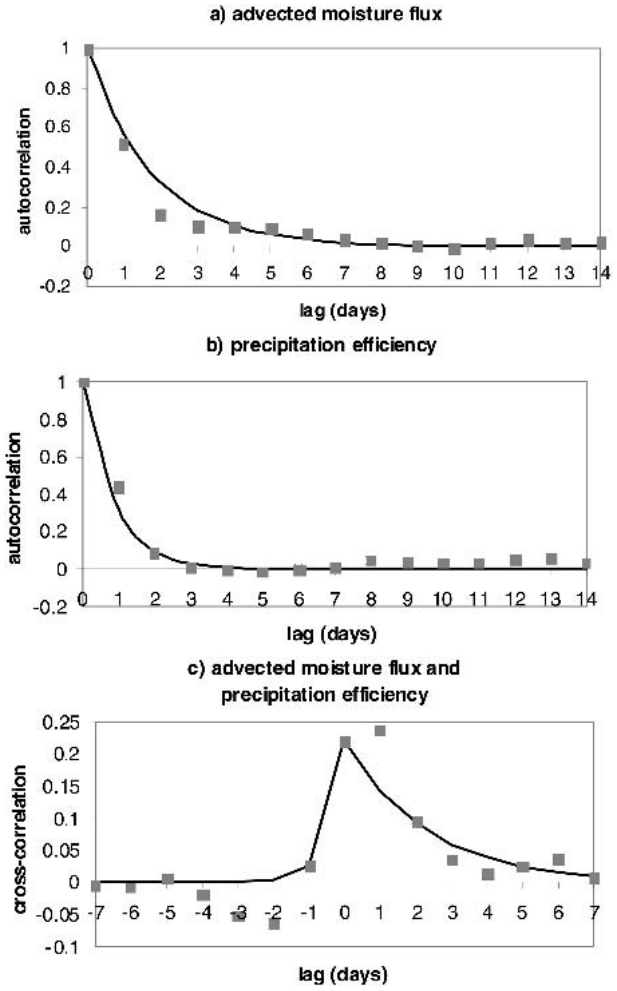

FIG. 6. Autocorrelation of daily (a) normalized advected moisture flux α, and (b) precipitation-efficiency h, and (c) cross correlation of α and h: (1983–93). Gray squares are observed values, and black curves are exponential fits.

mean, standard deviation and correlation time scale of the composite noise of 0.188, 1.83, and 0.89, respectively.

e. Precipitation-efficiency function

For the purposes of estimating ζ, η, and θ, the parameters of the precipitation-efficiency function, the daily values of h were aggregated to monthly values. A log–log plot of s versus h is presented in Fig. 7. The data have been divided into the five warmest months (May–September) and the seven coldest months (October–April). As one would expect for an energy-budget feedback, the correlation is strongest during the warm months, when precipitation is more often convectively generated. These months are also the core of growing season in Illinois, when vegetation draws moisture from the entire root zone, thereby increasing the dependency of the surface energy balance on the moisture throughout the root zone. The seasonality in the strength of the correlation between s and h is supported by the study of Findell and Eltahir (1997), which found a peak in correlation between soil moisture and lagged precipitation in Illinois during spring and summer months. The range of precipitation efficiency for the warm months in Fig. 7 is also comparable to the approximately two- to four-fold increases in precipitation efficiency that Schär et al. (1999) found between their July dry-soil and wet-soil simulations over domains encompassing France and central/eastern Europe.

We could use the regression results in Fig. 7 to parameterize the precipitation efficiency function with $\zeta = 0$. However, because of the seasonality in both the magnitude of h and the strength of the correlation between s and h, an alternative was used. Specifically, an optimization routine was used to minimize the sum of the squared errors (SSE) between the observed monthly values of h and those predicted by the equation for h. Three parameterizations of the precipitation efficiency function were developed corresponding to (29), (30), and (31). In the first case, θ was set equal to 2, in order to increase the analytical tractability of (29). The SSEs of the first two cases—those with precipitation-efficiency feedbacks—are identical to two significant figures, while the SSE of the third case—that with a constant h—is 20% greater, lending further support for including a dependency of h on s.

4. Results: Temporal variability of soil moisture

The analytical solutions for the steady-state PDFs of soil moisture corresponding to (29), (30), and (31) and their associated parameter values in Table 1 are plotted in Fig. 8. Because the analytical solutions were derived under the assumption of no surface runoff, the values used for the runoff parameters are those in the left-

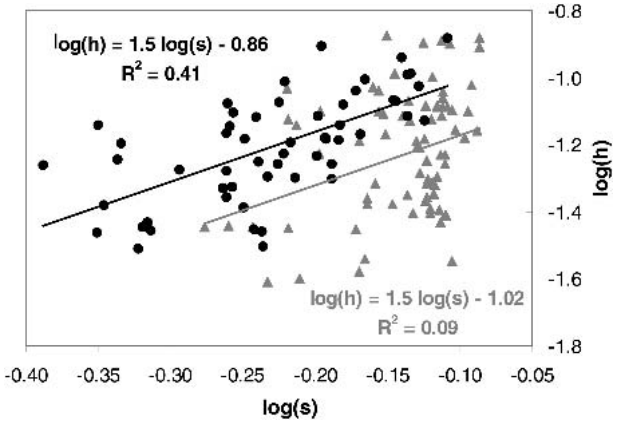

FIG. 7. Monthly average soil moisture vs precipitation efficiency (1983–93). Black circles are warm months/growing season (May–Sep). Gray triangles are cold months (Oct–Apr). Correspondingly colored lines and equations are regression results.

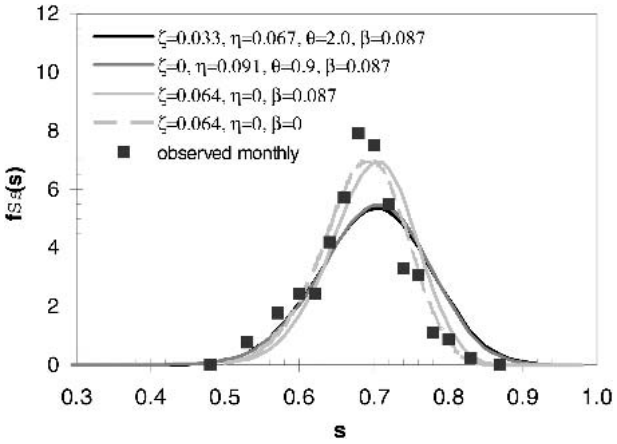

FIG. 8. Approximate analytical solutions of the Fokker–Plank equation for three parameterizations of the precipitation-efficiency function. The third parameterization is plotted both with and without precipitation recycling. Black squares are the PMF of "seasonless" observed monthly values (1983–2001).

hand column. The two solutions with precipitation-efficiency feedbacks ($\eta > 0$) are nearly identical, indicating that the two versions of $h(s)$ have similar form over the realized range of s. The variance of s for these two cases is 0.0053 and 0.0055. In contrast, about 40% less variance (=0.0034) is observable in the precipitation-recycling–only case ($\eta = 0$, $\beta > 0$). Finally, the PDF with no feedbacks at all ($\eta = 0$, $\beta = 0$) is also plotted. With the resulting removal of precipitation recycling, there is only a slight shift to the left of the PDF and an insignificant reduction in variance, indicating that precipitation recycling is not a major source of soil-moisture variability for the scale and climate of the study region. The variance in this case—that is, that without either precipitation recycling or precipitation-efficiency feedbacks—is entirely derived from the high-frequency variability in the input of atmospheric moisture and precipitation efficiency, as captured by the colored noise in the model.

For the purpose of comparison to the model results, we removed the seasonality in the observations of monthly average soil moisture by first standardizing them with the mean and standard deviation for the given month and then transforming them back with the overall mean and the average of the within-month standard deviations. The probability mass function (PMF) of the resulting values of s for all 227 months in the record is plotted in Fig. 8. While the variance of the precipitation-recycling-only case matches the variance of the observed PDF best, the model as a whole does a surprisingly good job of matching the observed variance, considering the physical simplicity of the model and the limits of the data. The lack of seasonality in the model and the difference in time scales are particularly significant limitations to comparing model results with observations. The longer averaging time of the observations is one reason to expect that their variance will be less than the model results. The connectivity of root-zone soil to the subsoil and groundwater—which have longer memory—may also contribute to the lower variance in the observations. The model in its present form does not capture this connectivity. The model results in Fig. 8 were also produced under the assumption of no surface runoff. As seen in the scaling analysis below, including surface runoff will further reduce the variance in the PDF.

For the purposes of confirmation of the approximate analytical solutions, PDFs for the first case (i.e., that with $\zeta = 0.033$, $\eta = 0.067$, and $\theta = 2.0$) are arrived at by two additional methods. The first case was chosen because it uses the most nonlinear form of the precipitation-efficiency function. The first method is numerical integration of (27). As can be seen in Fig. 9, the anticipated shift to the left by the approximate analytical solution (see the appendix) is virtually imperceptible. The second method of validating the analytical solution—as well as the SDE itself—is a 5000-yr simulation of (7) at a daily time step, with α and h generated stochastically according to (8), (9), and (10); γ_α and γ_h were simulated as a bivariate AR(1) process (e.g., Bras and Rodriguez-Iturbe 1985). The PMF of the resulting values of s is plotted in Fig. 9. Also plotted in Fig. 9 is a PMF of 30-day averages of the simulation results. The reduction in variance is only slight, indicating that the persistence in soil moisture is large enough that the monthly averaging time of observed soil moisture explains only a small part of the difference in variance between the observed PMF and the modeled PDFs in Fig. 8.

The final observation we make about the PDFs in Fig. 8 is that they are nearly symmetric and unimodal and, hence, exhibit no propensity for bimodality. They do possess a slight leftward skew, which is also evident

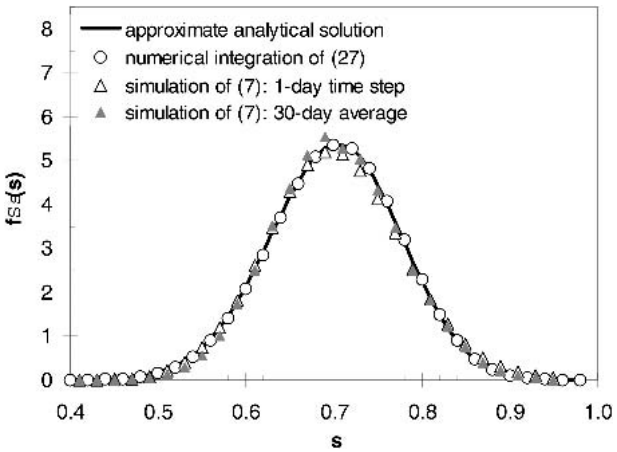

FIG. 9. Comparison of the approximate analytical solution of the PDF [Eq. (30)] with numerical integration of (27) and a stochastic simulation of (7). Parameter values for the precipitation-efficiency function are $\zeta = 0.033$, $\eta = 0.0067$, and $\theta = 2.0$.

in the observed PMF. With the white-noise model of Rodriguez-Iturbe et al. (1991), the transition to bimodality takes place with increasing variance in the noise. By extension, bimodality may be induced in our colored-noise model by increasing not only the variance but also the correlation time scale of the composite noise. It is expected that both would be a function of spatial scale. As spatial scale is increased, moisture fronts would reside longer in the region and hence both τ_α and τ_h should increase. In contrast, we expect ν_h and σ_α to decrease, as not only do moisture fronts reside longer in the region, but also the likelihood of multiple fronts being present at the same time within the region increases. Figure 10 shows the effect of proportional increases in τ_α, τ_h, and β. The latter parameter is also scaled because increasing the downwind length of the region would proportionally increase the contribution of evapotranspiration from within the region to the overall moisture flux. The other parameters in the model remain the same with the exception that the runoff parameters are those for the case of $r_s = 1$ (see Table 1) because, as discussed in the appendix, the inclusion of surface runoff is necessary for $s = 1$ to be a *prescribed boundary*. The effect on the PDFs of adding surface runoff is a decrease of about 15% in the variance and enhancement of the skewness. A final difference with the PDFs of Fig. 8 is that those of Fig. 10 were generated by numerical integration of (27)—as further discussed in the appendix, we assumed that τ was on the order of a few days to arrive at (28) and its analytical solutions, (29)–(31).

In all three parameterizations, as the correlation time scales are increased, a heavy skew to the left develops at the same time the mode shifts to the right. Bimodality develops only in the parameterization with $\zeta = 0$, which is the only one with a prescribed boundary at $s = 0$. The second mode is at $s = 0$, so it represents the unlikely case of precipitation ceasing. Furthermore, the mode develops between a scale factor of 10 and 15. Under the unlikely conditions of the correlation time scales increasing in proportion to the downwind length, and the variance of the noise remaining constant, the corresponding spatial scale is about 5000–7500 km—greater than the width of the United States at the latitude of Illinois and much greater than the scale at which the precipitation-efficiency feedback mechanisms are likely to operate. Therefore, soil-moisture feedbacks to precipitation alone are unlikely to induce bimodality in soil moisture at large regional-to-continental scales for midlatitude, semihumid climates.

The alternative possibility is that bimodality might occur at spatial scales smaller than the study region. As spatial scale decreases, and larger scales of atmospheric motion are lost, the variance of the noise is expected to increase. Figure 11 shows the effect of proportional increases in both ν_h and σ_α. Because the other parameter values and solution methodology are the same as in Fig. 10, the PDFs for a scale factor of one are the same. As the scale factor increases in Figs. 11a–d, a leftward skew and shift of the primary, wet mode to the right occur as in Fig. 10, although not as dramatically. In contrast to Fig. 10, a second, dry mode develops for both param-

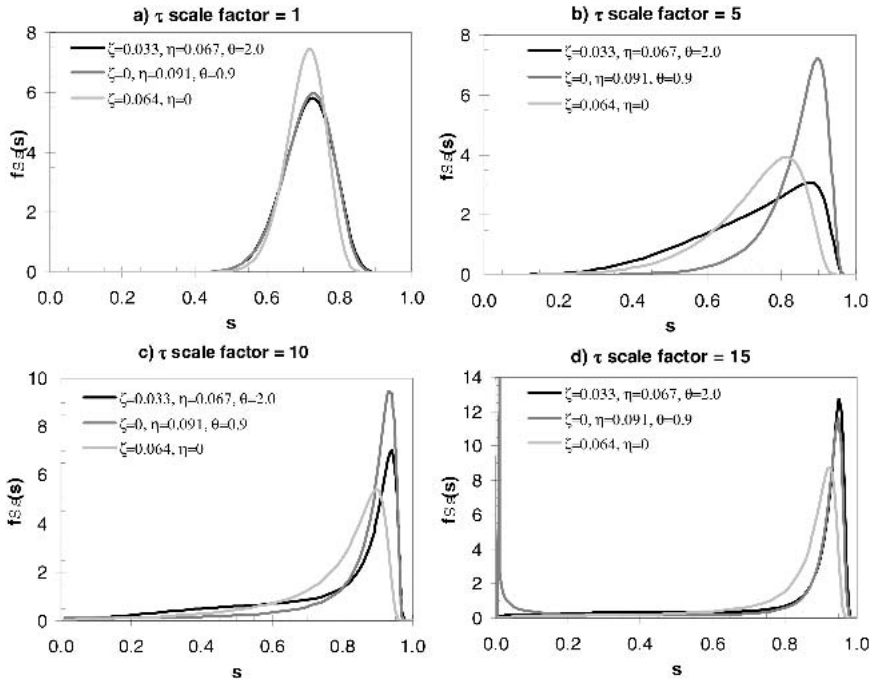

FIG. 10. The effect of increasing correlation time scales on the PDFs of soil moisture as might be manifested by increasing spatial scale.

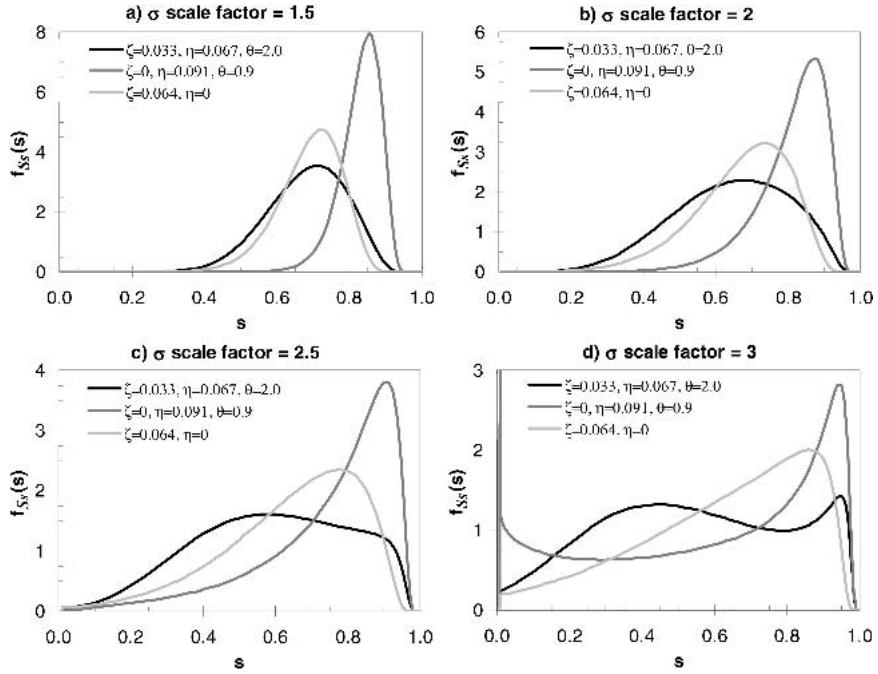

FIG. 11. The effect of increasing variance in the noise on the PDFs of soil moisture as might be manifested by decreasing spatial scale.

eterizations with precipitation-efficiency feedbacks. The dry mode in the parameterization with $\zeta = 0$ is more pronounced and quickly shifts to $s = 0$ as in Fig. 10. The soil-moisture feedbacks, as well as our assumption in the model of continuous precipitation, require at least a small regional spatial scale. Thus, there are limits to how large ν_h and σ_α can be. We are also limited in parameterizing smaller scales by the resolution of NCEP–NCAR reanalysis. At minimum we can calculate the standard deviation of α at a single grid point. Doing that for the grid point at the center of the study region produces a value of 0.71, only slightly larger than that calculated for the study region using all nine grid points. Therefore, reducing the spatial scale is also highly unlikely to produce bimodality.

5. Concluding remarks

Based on analysis with an SDE-based, large-scale water balance model, and detailed observations of relevant hydrologic and atmospheric variables, this study suggests that energy-budget feedbacks, as captured by a soil-moisture-dependent precipitation-efficiency function, are a substantial source of the temporal variability of soil moisture in the semihumid regions of the U.S. Midwest. On the other hand, precipitation recycling within a regional-scale domain does not contribute to atmospheric moisture flux sufficiently to have a significant impact on soil-moisture variability. Despite the significance of precipitation-efficiency feedbacks, they, along with precipitation recycling, are clearly not strong enough to induce a bimodal probability distribution in spatially averaged soil moisture, as other SDE-based studies (Rodriguez-Iturbe et al. 1991; Entekhabi et al. 1992; Wang et al. 1997) have suggested. Because the study focuses on a specific region of the United States, we do not prima facie dismiss the possibility that a feedback-induced, two-state dynamic exists elsewhere. However, the work of Koster et al. (2000) and others suggests that midlatitude, semihumid climates are where the impact of land surface feedbacks on the interannual variability of precipitation are the strongest relative to that of ocean–atmosphere teleconnections. We also do not dismiss the possibility that a two-state dynamic might exist in external drivers of the system with enough strength and persistence alone to produce bimodality in soil moisture.

In its present form, the model is a useful tool for examining the impact of the nonlinear dynamics of soil-moisture feedbacks to precipitation on the variability of soil moisture at the regional scale. In estimating parameter values for the study region, we have demonstrated that hydrometeorological fluxes—most of which have high-frequency temporal variability and are dependent on smaller-scale spatial heterogeneities—can be captured at regional scales over long averaging periods by empirical power functions of spatially averaged soil moisture. A key feature of the simplified representation of those fluxes is the use of a soil-moisture–dependent precipitation-efficiency factor. That a correlation exists between soil moisture and precipitation

efficiency over the study region was shown in section 3e. While that correlation does not prove a causal mechanism, both the existence of positive precipitation-efficiency feedbacks and the assumed strength of those feedbacks are supported by observational and modeling studies of the region (Findell and Eltahir 1997; Zheng and Eltahir 1998; Brown and Arnold 1998; Pal and Eltahir 2001) and similar climates of Europe (Schär et al. 1999). Greater confidence in the conclusions of this study depends on further elucidation of the mechanisms and magnitudes of precipitation–efficiency feedbacks, especially with regards the extent to which they are dependent on regional-scale averages of soil moisture.

In a forthcoming paper, it will be shown that the model also does a good job of reproducing the persistence and interannual variability in the soil-moisture observations for Illinois. We will also examine the persistence and interannual variability of precipitation, as well as use of the model to resolve the relative contributions of land- surface feedbacks, ocean–atmosphere teleconnections, and chaotic atmospheric dynamics to the interannual variability of the water balance.

Acknowledgments. This work was partially supported by the National Institute for Global Environmental Change through the U.S. Department of Energy (Cooperative Agreement DE-FC03-90ER61010).

APPENDIX

Analysis of Solution Boundaries

While soil moisture is physically limited to the interval $s \in [0,1]$ in the real world, it may not be mathematically in the model. Both the drift and diffusion terms determine the boundaries of the solution of the FPE. We first consider the significance of the drift term. If the soil were ever to become either completely saturated (i.e., $s = 1$) or dry to its residual moisture limit (i.e., $s = 0$), it should move back to the interior of the interval; $s = 0$ and $s = 1$ would then be *entrance boundaries*, and it would be necessary that $A(0) > 0$ and $A(1) < 0$ (Gardiner 1985). In the denominators of (25a) and (25b),

$$\delta(s)\frac{d}{ds}\left[\frac{\Delta(s)}{\delta(s)}\right] = s^{-1}\left[a\beta s^{\varepsilon}(\zeta + \eta s^{\theta})(1 - s^{\rho_s}) - \varepsilon e_p s^{\varepsilon} - \rho_g k s^{\rho_g} + \frac{\eta\theta s^{\theta}(e_p s^{\varepsilon} + k s^{\rho_g})}{\zeta + \eta s^{\theta}} - \frac{\rho_s s^{\rho_s}(e_p s^{\varepsilon} + k s^{\rho_g})}{1 - s^{\rho_s}}\right], \quad \text{(A1)}$$

where r_s has been set equal to one. Thus, for any set of nonnegative parameter values with ε and ρ_g greater than 1,

$$\lim_{s \to 0} \delta(s)\frac{d}{ds}\left[\frac{\Delta(s)}{\delta(s)}\right] = 0 \quad \text{(A2)}$$

and $A(0) = \Delta(0)$, which is greater than zero as long as ζ is greater than zero. On the other hand,

$$\lim_{s \to 1} \delta(s)\frac{d}{ds}\left[\frac{\Delta(s)}{\delta(s)}\right] = -\infty. \quad \text{(A3)}$$

Consequently $A(1) = 0$, and therefore $s = 1$ is actually a *natural boundary* at which s would tend to remain. Equation (A3) comes about only because we set r_s to unity in (A1). However, if the diffusion term goes to zero near $s = 1$, the boundary cannot be reached and is also termed a *prescribed boundary* (Gardiner 1985). The drift and diffusion terms share the same denominator and $\delta(1) = 0$, so (25b) does in fact go to zero near $s = 1$. From the standpoint of a physically realistic PDF, a prescribed boundary is desirable because it ensures that the PDF will be zero at that boundary. From (16c), we see that $s = 0$ is a prescribed boundary only when $\zeta = 0$. With $\zeta = 0$, the drift term also goes to zero, and thus $s = 0$ also becomes a natural, prescribed boundary. The physical implication for $s = 0$ is the cessation of all fluxes to and from the soil. This would be expected of evapotranspiration and groundwater runoff, but unlikely to happen to precipitation. However, the precipitation efficiency may still be well approximated over the realized range of s with $\zeta = 0$ (see section 3e).

To argue for a simpler, but approximate solution of (27a)–(27b), we examine the form of (A1). We have already established that (A1) ranges from 0 to $-\infty$; plotting it with example parameter sets reveals that the asymptote becomes sharper as ρ_s increases. This behavior is such that, if we assume that τ is on the order of a few days or less, and that the surface runoff ratio is small—generally, a reasonable assumption for all but the most humid climates and steep terrain—we can approximate the denominators in (25a)–(25b) as 1. Because the overestimation in the drift term created by this approximation worsens as s approaches one, we expect that the overall effect will be to shift probability mass to the left—an effect almost imperceptible in the analytical solution as compared to the exact numerical integration in Fig. 9. The approximation also necessitates re-evaluation of the boundary conditions. The nature of the boundary at $s = 0$ remains unchanged. On the other hand, $\Delta(1) < 1$, and so $s = 1$ becomes an *entrance boundary*. The prescribed status of $s = 1$ still depends on $r_s = 1$. However, setting r_s equal to zero is also desirable for simplifying the evaluation of the integral in (28). Based on a comparison between the PMF for the numerical simulation and the PDFs in Fig. 9, a consequence of the absence of a prescribed boundary at $s = 1$ may be a slight shift of the PDF to the right. Otherwise, it does not appear to be a problem for the

given parameter values. However, the much larger values of the correlation time scales and noise variances used in the scaling analysis do create unrealistic behavior at $s = 1$ in the approximate analytical solutions—hence the reason they were not used in that analysis.

REFERENCES

Benjamin, J. R., and C. A. Cornell, 1970: *Probability, Statistics, and Decision for Civil Engineers*. McGraw-Hill, 684 pp.

Bras, R. L., and I. Rodriguez-Iturbe, 1985: *Random Functions and Hydrology*. Dover, 559 pp.

Brooks, R. H., and A. T. Corey, 1966: Properties of porous media affecting flow. *J. Irrig. Drain. Div.,* **92** (2), 61–88.

Brown, M. E., and D. L. Arnold, 1998: Land-surface–atmosphere interactions associated with deep convection in Illinois. *Int. J. Climatol.,* **18,** 1637–1653.

Brubaker, K. L., D. Entekhabi, and P. S. Eagleson, 1993: Estimation of continental precipitation recycling. *J. Climate,* **6,** 1077–1089.

Budyko, M. I., 1974: *Climate and Life*. Academic Press, 508 pp.

Charney, J., J. Q. Quirk, S.-H. Chow, and J. Kornfield, 1977: A comparative study of effects of albedo change on drought in semi-arid regions. *J. Atmos. Sci.,* **34,** 1366–1385.

Daly, C., R. P. Neilson, and D. L. Phillips, 1994: A statistical-topographic model for mapping climatological precipitation over mountainous terrain. *J. Appl. Meteor.,* **33,** 140–158.

Eltahir, E. A. B., 1998: A soil moisture–rainfall feedback mechanism, 1. Theory and observations. *Water Resour. Res.,* **34**, 765–776.

——, and P. Yeh, 1999: On the asymmetric response of aquifer water level to floods and droughts in Illinois. *Water Resour. Res.,* **35**, 1199–1217.

Entekhabi, D., I. Rodriguez-Iturbe, and R. L. Bras, 1992: Variability in large-scale water balance with land surface–atmosphere interaction. *J. Climate,* **5,** 798–813.

Findell, K. L., and E. A. B. Eltahir, 1997: An analysis of the soil moisture–rainfall feedback mechanism, based on direct observations from Illinois. *Water Resour. Res.,* **33**, 725–735.

Gardiner, C. W., 1985: *Handbook of Stochastic Methods for Physics, Chemistry and the Natural Sciences*. 2d ed. Springer-Verlag, 442 pp.

Higgins, R. W., W. Shi, E. Yarosh, and R. Joyce, cited 2000: *Improved United States Precipitation Quality Control System and Analysis.* NCEP/Climate Prediction Center Atlas 7, National Oceanic and Atmospheric Administration, National Weather Service. [Available online at http://www.cpc.ncep.noaa.gov/research_papers/ncep_cpc_atlas/7/.]

Hobbins, M. T., J. A. Ramírez, T. C. Brown, and L. H. J. M. Claessens, 2001: The complementary relationship in estimation of regional evapotranspiration: The complementary relationship areal evapotranspiration and advection-aridity models. *Water Resour. Res.,* **37**, 1367–1388.

Hollinger, S. E., and S. A. Isard, 1994: A soil moisture climatology of Illinois. *J. Climate,* **7,** 822–833.

Høyrup, M., 1996: The influence of passed-diffused laser light on three-level atoms. M.S. thesis, Institute of Physics and Astronomy, Aarhus University, 121 pp.

Jackson, R. B., J. Canadell, J. R. Ehleringer, H. A. Mooney, O. E. Sala, and E. D. Schulze, 1996: A global analysis of root distributions for terrestrial biomes. *Oecologia,* **108,** 389–411.

Kalnay, E., and Coauthors, 1996: The NCEP/NCAR 40-Year Reanalysis Project. *Bull. Amer. Meteor. Soc.,* **77**, 437–471.

Koster, R. D., M. J. Suarez, and M. Heiser, 2000: Variance and predictability of precipitation at seasonal-to-interannual timescales. *J. Hydrometeor.,* **1,** 26–46.

Pal, J. S., and E. A. B. Eltahir, 2001: Pathways relating soil moisture conditions to future summer rainfall within a model of the land–atmosphere system. *J. Climate,* **14,** 1227–1242.

Penman, H. L., 1948: Natural evaporation from open water, bare soil and grass. *Proc. Roy. Soc. London,* **A193,** 120–145.

Pielke, R. A., and X. Zeng, 1989: Influence on severe storm development of irrigated land. *Natl. Wea. Dig.,* **14,** 16–17.

Robock, A., K. Y. Vinnikov, G. Srinivasan, J. K. Entin, S. E. Hollinger, N. A. Speranskaya, S. Liu, and A. Namkhai, 2000: The Global Soil Moisture Data Bank. *Bull. Amer. Meteor. Soc.,* **81,** 1281–1299.

Rodell, M., and J. S. Famiglietti, 2001: An analysis of terrestrial water storage variations in Illinois with implications for the Gravity Recovery and Climate Experiment (GRACE). *Water Resour. Res.,* **37**, 1327–1339.

Rodriguez-Iturbe, I., D. Entekhabi, and R. L. Bras, 1991: Nonlinear dynamics of soil moisture at climate scales, 1. Stochastic analysis. *Water Resour. Res.,* **27**, 1899–1906.

Savenije, H. H. G., 1995: New definitions for moisture recycling and the relationship with land-use changes in the Sahel. *J. Hydrol.,* **167,** 57–78.

Schär, C. D., D. Lüthi, U. Beyerle, and E. Heise, 1999: The soil–precipitation feedback: A process study with a regional climate model. *J. Climate,* **12,** 722–741.

Shuttleworth, W. J., 1993: Evaporation. *Handbook of Hydrology*, D. R. Maidment, Ed., McGraw-Hill, 4.1–4.53.

Wang, J., R. L. Bras, and D. Entekhabi, 1997: Structure in fluctuations of large-scale soil moisture climate due to external random forcing and internal feedbacks. *Stochastic Hydrol. Hydraul.,* **11,** 95–114.

Woodruff, J. F., and J. D. Hewlett, 1970: Predicting and mapping the average hydrologic response for the eastern United States. *Water Resour. Res.,* **6**, 1312–1326.

Yeh, P. J.-F., M. Irizarry, and E. A. B. Eltahir, 1998: Hydroclimatology of Illinois: A comparison of monthly evaporation estimates based on atmospheric water balance and soil water balance. *J. Geophys. Res.,* **103** (D16), 19 823–19 837.

Zheng, X., and E. A. B. Eltahir, 1998: A soil moisture–rainfall feedback mechanism, 2. Numerical experiments. *Water Resour. Res.,* **34**, 777–785.